Sequence of Ligand Binding and Structure Change in the Diphtheria Toxin Repressor upon Activation by Divalent Transition Metals†

Vijayaraghavan Rangachari,‡ Vedrana Marin,§ Ewa A. Bienkiewicz,‡ Maria Semavina,‡ Luis Guerrero,‡ John F. Love,|| John R. Murphy,|| and Timothy M. Logan*,‡,§,⊥

Kasha Laboratory, Institute of Molecular Biophysics, Florida State University, Tallahassee, Florida 32306, Department of Chemistry and Biochemistry, Florida State University, Tallahassee, Florida 32306, Evans Department of Clinical Research and Department of Medicine, Boston University School of Medicine, Boston University, Boston, Massachusetts 02118, and National High Magnetic Field Laboratory, 1800 East Paul Dirac Drive, Tallahassee, Florida 32310

Received October 8, 2004; Revised Manuscript Received February 9, 2005

ABSTRACT: The diphtheria toxin repressor (DtxR) is an Fe(II)-activated transcriptional regulator of iron homeostatic and virulence genes in *Corynebacterium diphtheriae*. DtxR is a two-domain protein that contains two structurally and functionally distinct metal binding sites. Here, we investigate the molecular steps associated with activation by $Ni(II)Cl_2$ and $Cd(II)Cl_2$. Equilibrium binding energetics for Ni(II) were obtained from isothermal titration calorimetry, indicating apparent metal dissociation constants of 0.2 and 1.7 μM for two independent sites. The binding isotherms for Ni(II) and Cd(II) exhibited a characteristic exothermic−endothermic pattern that was used to infer the metal binding sequence by comparing the wild-type isotherm with those of several binding site mutants. These data were complemented by measuring the distance between specific backbone amide nitrogens and the first equivalent of metal through heteronuclear NMR relaxation measurements. Previous studies indicated that metal binding affects a disordered to ordered transition in the metal binding domain. The coupling between metal binding and structure change was investigated using near-UV circular dichroism spectroscopy. Together, the data show that the first equivalent of metal is bound by the primary metal binding site. This binding orients the DNA binding helices and begins to fold the N-terminal domain. Subsequent binding at the ancillary site completes the folding of this domain and formation of the dimer interface. This model is used to explain the behavior of several mutants.

With few exceptions, ferrous iron [Fe(II)] is required for growth and survival, but the concentration of Fe(II) must be carefully regulated (*1*). High concentrations of ferrous iron generate oxidative damage when it is oxidized to the ferric form, whereas low concentrations prevent the normal functioning of a variety of cellular processes. Mammalian cells store ferric iron and reduce it to the ferrous form as needed. On the other hand, bacteria generally do not store ferric or ferrous iron and directly utilize ferrous iron taken into the cell. This direct dependence on environmental Fe(II) presents special problems for pathogenic bacteria, which must compete for available iron with the host cells. As one solution to this problem, many bacteria link virulence to metal availability (*2*, *3*). Normally, virulence gene expression is repressed in the presence of sufficient bacterial iron levels. However, when bacterial iron stores drop, virulence gene expression is derepressed. The virulence factors kill neighboring host cells, making their stored iron available to the pathogen.

Fe(II) sensing and homeostasis in many Gram-positive bacteria are linked to virulence by a family of proteins related to the diphtheria toxin repressor (DtxR),[1] which was initially isolated as the iron-dependent regulator of diphtheria toxin expression in *Corynebacterium diphtheriae* (*4*). DtxR has subsequently been shown to regulate other genes involved in iron uptake and utilization. IdeR, the iron-dependent repressor from *Mycobacterium tuberculosis* and the closest DtxR homologue (*5*), is proposed to regulate the expression of more than 45 different gene products (*6*), functioning in some cases as a repressor and in others as an activator of gene expression. To date, more than 30 DtxR homologues have been identified in Gram-positive, Gram-negative, and archae bacteria, including *Treponema pallidum* (*7*), *Streptococcus gordonii* (*8*), *Bacillus subtilis* (*9*), and many others.

† Supported by the American Heart Association (Grant 0225339B to V.R.), the National Institutes of Health (Grant R01 AI021628-20 to J.R.M.), the National High Magnetic Field Laboratory, and the Florida State University Research Foundation (T.M.L.).

* To whom correspondence should be addressed: 502 MBB 4380, Kasha Laboratory, Florida State University, Tallahassee, FL 32306-4380. Phone: (850) 644-8979. Fax: (850) 644-7244. E-mail: logan@sb.fsu.edu.

‡ Institute of Molecular Biophysics, Florida State University.

§ Department of Chemistry and Biochemistry, Florida State University.

|| Boston University.

⊥ National High Magnetic Field Laboratory.

[1] Abbreviations: DtxR, diphtheria toxin represssor; IdeR, iron-dependent repressor from *M. tuberculosis*; DtxRΔSH3, residues 1−142 of DtxR; Pr segment, residues 125−135 of DtxR; ITC, isothermal titration calorimetry; HSQC, heteronuclear single-quantum coherence spectroscopy; R_{1e}, enhancement in the longitudinal relaxation rate caused by the paramagnetic metal center.

10.1021/bi047825w CCC: $30.25
Published on Web 03/25/2005

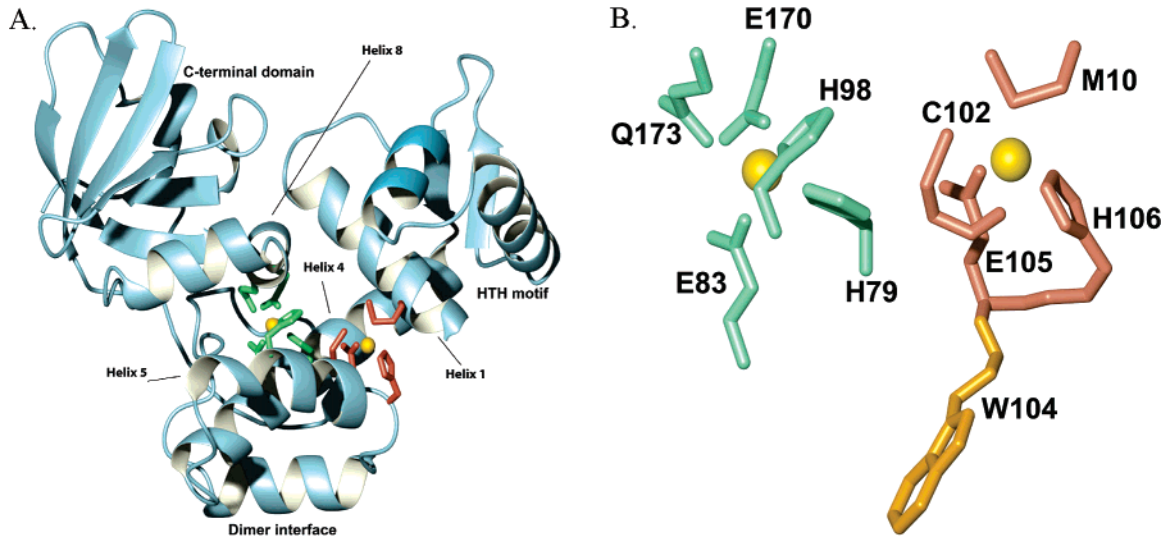

FIGURE 1: Metal binding sites in Co(II)-activated DtxR [PDB entry 1c0w (*18*)]. The primary site residues are colored brown and the ancillary site residues green.

The central role played by DtxR and its homologues in bacterial survival has generated interest in the molecular mechanisms by which metal binding effects gene regulation in this family of proteins. This has led to the identification of a hyperactive mutant of DtxR that represses target genes at much lower metal concentrations than the wild-type protein (*10*) and to the identification of peptide activators of DtxR (*11*). The introduction of the hyperactive DtxR mutant into virulent *M. tuberculosis* reduces virulence in mouse models (*12*), further emphasizing the importance of understanding the activation of these proteins.

DtxR contains two structurally (*13*−*15*) and functionally (*16*) distinct metal binding sites in the larger of its two domains (the N-terminal or N domain; residues M1−V123). The primary metal binding site (Figure 1) is formed by the side chains of residues M10, C102, E105, and H106 and the backbone carbonyl of C102. Mutation of any of these residues to alanine completely inactivates the repressor (*16*). The ancillary site contains the side chains of residues H79, E83, and H98 from the N domain, and residues E170 and Q173 from the C-terminal domain (*17*−*19*) (Figure 1). Mutations in the ancillary site reduce repressor activity to varying degrees, but not more than 50% (*16*, *20*). The C-terminal domain (A147−L226) is structurally homologous to eukaryotic SH3 domains (*17*−*19*). Structurally, the N domain of DtxR exists as a molten globule ensemble of conformers in the absence of metal. This state has a high helical character and is weakly dimeric, but lacks fixed tertiary structure. Metal binding effects a disordered to ordered structural transition that folds the N domain (*21*), increases the affinity for the dimer (*22*), and orients the DNA binding helices for binding to the *tox* promoter/operator site (*13*, *15*).

DtxR binds to and becomes activated for DNA binding in vitro by other metals in the following relative order: Fe(II) ∼ Ni(II) > Co(II) ≫ Mn(II) (*22*−*24*); Zn(II) and Cd(II) are also bound by and activate DtxR (*25*), although a quantitative comparison of activation by Zn(II) and Cd(II) metals has not been published. Structural studies of DtxR activation have utilized Fe(II), Co(II), Mn(II), Cd(II) (*13*, *17*, *26*), and Ni(II) (*15*, *16*). Although the earlier studies were complicated by oxidation of the C102 thiol, there appears to be very little difference in the structures of the metal-bound state of DtxR, suggesting that these different metals can be used to probe the activation process.

In this work, we focus on characterizing the energetics and sequence of metal binding to DtxR, using Ni(II), Cd(II), and Mn(II). Early studies showed that the binding affinity for Ni(II) was in the low micromolar range. However, one study exhibited rectangular hyperbolic binding (*27*), whereas a second study showed a partially sigmoidal binding curve (*28*). A more recent study, performed with rigorously demetalated protein preparations, indicated 2 equiv of metal bound by DtxR with an equilibrium dissociation constant in the low micromolar range for Ni(II) (*22*), but the study was unable to distinguish binding the two separate sites. Here, isothermal titration calorimetry (ITC) was used to investigate binding the chloride salts of Ni(II) and Cd(II) metals. The data indicated multiple binding sites with apparent binding affinities in the nano- to micromolar range. Furthermore, metal binding yielded a unique temporal profile that was dissected using site-specific mutants in the primary and ancillary metal binding sites to reveal the specific sequence of metal binding. These results were extended by the use of heteronuclear NMR relaxation studies. The connection between metal binding and structural ordering was investigated by use of near-UV circular dichroism (CD) spectroscopy. Together, the results of this study extend the description of metal binding energetics in DtxR and demonstrate a specific sequence of events leading to the activation of the aporepressor.

MATERIALS AND METHODS

Construction of Mutant DtxR Genes. The H79A and E83A ancillary site DtxR mutants were generated previously (*16*) and used without modification. The M10A mutant (*16*) was subcloned from an expression system based on the pROM plasmid (*29*) into pET-11b by digestion of the PCR-amplified product with *Nde*I and *Bam*HI restriction endonucleases, followed by ligation into pET-11b digested with the same enzymes. The C102A mutation (*16*) was introduced into the wild-type DtxR gene via the Quik-Change mutagenesis kit

(Stratagene, La Jolla, CA) using forward and reverse primers of 5′-GTTCACGATGAAGCCGCCCGATGGGAACAT-GTCATG-3′ and 5′-CATGACATGTTCCCATCGGGCG-GCTTCATCGTGAAC-3′, respectively. The generation of DtxRΔSH3 (encoding residues M1−N142) was described previously (*30*) and used without modification. The sequence of all constructs used in this work was confirmed by direct sequencing of the expression plasmids.

Protein Purification. Cells were grown at 37 °C in LB to an optical density (OD) of ∼0.6 at 600 nm, induced by isopropyl thiogalactoside (final concentration of 1 mM) and harvested by centrifugation 3.5 h after induction. Cell pellets were resuspended in 50 mM Tris buffer at pH 8.0 (buffer A), lysed using a microfluidizer (Microfluidics Corp., Newton, MA) according to the manufacturer's instructions, and clarified by centrifugation. Protein concentrations were measured spectrophotometrically in the presence of 6 M urea at 280 nm (*31*) using a calculated extinction coefficient of 8250 cm^{-1} M^{-1} (www.expasy.org).

DtxR. The clarified cell lysis supernatant was chromatographed over a freshly charged nickel affinity column that was pre-equilibrated with buffer A. Fractions containing DtxR were concentrated and chromatographed on an anion exchange column (Q-Sepharose) pre-equilibrated in buffer A. DtxR was eluted using a linear gradient of NaCl between 0.22 and 0.27 M NaCl. The fractions were pooled, exchanged into 10 mM HEPES (pH 5.5) containing 2 M NaCl and 3 M urea, and chromatographed using a phenyl-Sepharose hydrophobic affinity column (Amersham Biosciences). DtxR eluted in two different fractions corresponding to the monomeric and disulfide-linked dimeric protein using a linear gradient of 0 to 2 M NaCl. Both fractions were pooled, concentrated, and dialyzed extensively against Chelex-treated 10 mM HEPES (pH 6.85) (see below).

DtxR M10A and C102A. The clarified cell lysate was directly loaded on the Q-Sepharose anion exchange column. M10A and C102A eluted at 0.25 and 0.28 M NaCl, respectively. The remainder of the purification was identical to that of wild-type DtxR except that C102A eluted in the flow-through on the hydrophobic affinity column.

DtxR H79A and E83A. These mutant proteins formed inclusion bodies when expressed. Therefore, the cell lysis pellet was resuspended in buffer A containing 6 M urea and centrifuged to pellet insoluble material. The supernatant was dialyzed against buffer A to remove urea and refold the protein prior to purification as described for wild-type DtxR.

DtxRΔSH3. The cell lysate in buffer A was loaded directly on the Q-Sepharose anion exchange column, with DtxRΔSH3 eluting between 40 and 80 mM NaCl. The rest of the purification proceeded as for wild-type DtxR.

Reduction and Demetalation. The C102 thiol of apoDtxR oxidizes slowly, but metal binding effectively prevents oxidation. Prior to metal binding experiments, all proteins were freshly reduced using a 150-fold excess of dithiothreitol (DTT) at 37 °C for 1 h, and exchanged into 10 mM HEPES (pH 6.8) using a desalting column. Reoxidation of the thiol occurs slowly over the course of 5−10 h at room temperature. The concentration of free thiol was determined using Ellman's reagent before and after ITC and CD experiments.

Preparation of Glassware and Solutions. Glassware and buffers were rigorously cleaned and demetalated. Glassware was soaked in 10% nitric acid overnight and exhaustively rinsed with deionized water. Buffer solutions were made using deionized water, and dry Chelex resin (50 g/L) was added with stirring overnight to remove trace metal contaminants. The solution was then filtered using a 0.22 μm filter into dry, acid-treated glassware.

Isothermal Titration Calorimetry. ITC experiments were performed using a VP-ITC microcalorimeter (Microcal Inc., Northampton, MA) at 25 °C. Protein solutions were exhaustively dialyzed against Chelex-treated buffer B, and the dialysate was used to generate the metal stock solutions. All solutions were degassed for 10 min prior to each experiment. Titrations were performed as 50 injections (4 μL each) of a 1.5 mM metal stock solution into a 25 μM protein solution in the sample cell (1.545 mL) of the calorimeter. DtxRΔSH3 (35 μM) was titrated with a 60-fold excess of metal as 26 injections (4 μL each). Each metal injection required 8 s with a 300 s relaxation interval between successive injections. All titrations were corrected by subtracting the heat of dilution obtained from the titration of metal into protein-free buffer solutions. These corrections and subsequent curve fitting were performed using Origin 7.0 provided by the manufacturer.

Circular Dichroism. Near-UV CD experiments were performed on an AVIV-202 CD spectropolarimeter (Proterion Corp., Piscataway, NJ) at 25 °C. The filtered protein stock was diluted to the desired concentration (25 μM) in 10 mM HEPES buffer (pH 6.8) containing metal at the final concentration. Samples were equilibrated for 1 h at 4 °C prior to data collection. A 1 cm path length quartz microcuvette was used for all spectra. Spectra were collected from 325 to 250 nm in 0.2 nm increments with 4 s averaging per increment. Three independent scans were collected for each protein sample (and for each buffer with metal), averaged, corrected for absorption by the buffer, and normalized for protein concentration. All spectral processing was performed using software provided by the manufacturer.

NMR Spectroscopy. Wild-type and mutant DtxR proteins were uniformly labeled with ^{15}N in minimal medium supplemented with 1 g/L $[^{15}N]NH_4Cl$ (Cambridge Isotope Laboratories, Cambridge, MA) and purified as described above. Samples of metal-bound DtxR were prepared by addition of $Mn(II)Cl_2$ or $Cd(II)Cl_2$ from freshly prepared 500 mM stock solutions at the desired stoichiometric ratio. Heteronuclear single-quantum coherence (HSQC) spectra and longitudinal relaxation times were measured at 30 °C using standard experiments (*32*, *33*) on a 720 MHz Varian Inova console. Spectral parameters were 12 001 and 2650 Hz sweep widths digitized by 1024 and 200 complex points in the ^1H and ^{15}N dimensions, respectively. Spectra were processed using nmrPipe (*34*) and analyzed using NMRView (*35*). Longitudinal ^{15}N relaxation delay times of 10, 140 (twice), 240, 370, 530 (twice), 760, and 1160 ms were recorded. Duplicate spectra were used to estimate the measurement error. Normalized resonance intensities were fitted to a single-exponential decay. The enhancement in longitudinal relaxation rate due to paramagnetic Mn(II), $R_{1,e}$, was determined from the difference in R_1 values of Mn(II)- and Cd(II)-bound DtxR. Distances were calculated using the Solomon−Bloembergen equation

$$R_{1,e} = \frac{2}{15}\left(\frac{\mu_0}{4\pi}\right)^2 \frac{\gamma_N^2 g_e^2 \mu_B^2 S(S+1)}{r^6} \times \left[\frac{7\tau_c}{1+(\omega_e\tau_c)^2} + \frac{3\tau_c}{1+(\omega_e\tau_c)^2}\right]$$

where ω_N and ω_e represent the nitrogen and electron Larmor frequencies, respectively, r is the nitrogen−metal distance, and τ_c is the correlation time for the dipolar coupling determined as

$$\tau_c^{-1} = \tau_e^{-1} + \tau_r^{-1} + \tau_m^{-1}$$

where τ_e, τ_r, and τ_m are the electron, rotational, and exchange correlation times, respectively. Other symbols have their standard meanings and values (*36*).

Mobility Shift Assays. Electrophoretic mobility assays were performed essentially as described previously (*23*, *24*). All protein samples initially contained a 10-fold molar ratio of Ni(II), and additional metal was added upon addition of DNA. All electrophoresis buffers contained 1 mM Ni(II)Cl_2. Protein (2 μM) was mixed with DNA (90 nM), incubated for 20 min at room temperature, and electrophoresed for 20 min at 200 V in a 6% acrylamide prerun gel equilibrated in Tris-borate buffer containing 1 mM Ni(II)Cl_2. Gels were stained with SYBR Gold (Molecular Probes, Eugene, OR) and visualized using a TYPHOON scanner.

RESULTS

Metal Binding by Wild-Type DtxR. Figure 2 shows the instantaneous heat evolution associated with titration of wild-type DtxR by Ni(II)Cl_2 or Cd(II)Cl_2. Binding either Ni(II) or Cd(II) is initially strongly exothermic followed by an endothermic phase prior to saturation at approximately 4 equiv of metal. The magnitude of the exothermic and endothermic heat evolution is greater for Cd(II) binding than for Ni(II) binding, but the overall pattern is similar. Titrations performed at protein concentrations from 3 to 60 μM at the same temperature had little effect on the overall pattern and relative amplitudes of the different portions of the binding isotherms.

A potential complication when interpreting the binding isotherms arises from the slow oxidation of the thiol group on C102. Disulfide-linked dimers are readily formed during purification, resulting in an inactive protein (*37*). To ensure complete reduction of C102, all proteins were reduced with excess dithiothreitol for 60 min at 37 °C and unreacted thiol was removed via buffer exchange. Incomplete reduction or residual thiol contamination was readily apparent in the binding isotherms, and data from these samples were not considered further. A final complication stems from possible metal binding by the SH3 domain, as observed in a recent crystal structure of Co(II)-activated IdeR (*38*). Addition of Ni(II)Cl_2 to an isolated SH3 domain construct (residues 144−226) showed weak binding of 1 equiv of metal with an equilibrium dissociation constant K_D of ~40 μM (not shown).

Metal Binding by Ancillary Site Mutants. In an attempt to assign the thermodynamic binding sites identified from the calorimetry data with the physical binding sites identified from genetic and structural analysis of DtxR, metal binding by various DtxR mutants was investigated. Figure 3 shows

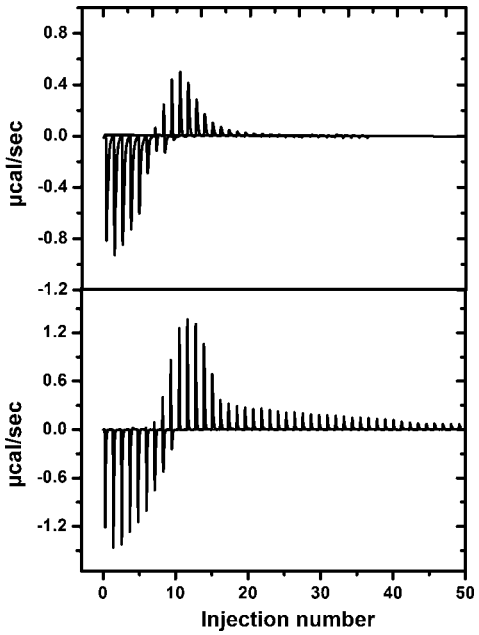

FIGURE 2: Blank-corrected instantaneous heats evolved upon titration of wild-type DtxR with Ni(II)Cl_2 (top) and Cd(II)Cl_2 (bottom).

the instantaneous heat evolutions associated with titrating Ni(II) or Cd(II) into DtxRΔSH3 (*20*) and the ancillary site mutants, H79A and E83A (*16*), respectively. All three proteins show a single exothermic binding process that saturates at roughly 1 equiv of added metal, indicating that metal binding at the ancillary site was substantially weakened in these mutants. Titration with Cd(II)Cl_2 resulted in aggregation and some precipitation as evidenced by the sample turbidity observed at the end of titrations. This process probably accounts for the nonsaturating endothermic heats observed at high metal:protein ratios. Metal-induced aggregation was not observed when titrating with Ni(II)Cl_2.

Metal Binding by Primary Site Mutants. Figure 4 shows the instantaneous heat evolutions obtained upon titration of Ni(II) or Cd(II) into C102A and M10A mutants (*16*) of DtxR. When titrated with $NiCl_2$, M10A exhibited a strong exothermic binding profile that saturated by the 15th injection, followed by a second exothermic binding that saturated after 26 injections. In response to increasing Ni(II) concentrations, C102A exhibited an exothermic binding process that saturated by the fourth injection followed by a second exothermic binding process that saturated at the 16th injection. On the other hand, titrating either of these mutants with Cd(II) yielded an initially exothermic binding process that became endothermic before saturation. Cd(II)-induced aggregation of both M10A and C102A was noted.

DNA Binding by DtxR and Metal Binding Mutants. Figure 5 compares the DNA binding ability of wild-type DtxR with that of the ancillary and primary site mutants. In the presence of saturating Ni(II)Cl_2, DtxRΔSH3 is able to bind and shift a high-affinity DNA sequence related to the *tox* promoter (*23*, *24*) similar to the wild-type protein. H79A shows a weakened ability to bind DNA, whereas C102A and M10A are incapable of binding DNA.

Metal-Induced Folding of DtxR. We previously established that metal binding induces a folding transition involved in the activation of DtxR (*21*). Far-UV CD spectra of the apo-

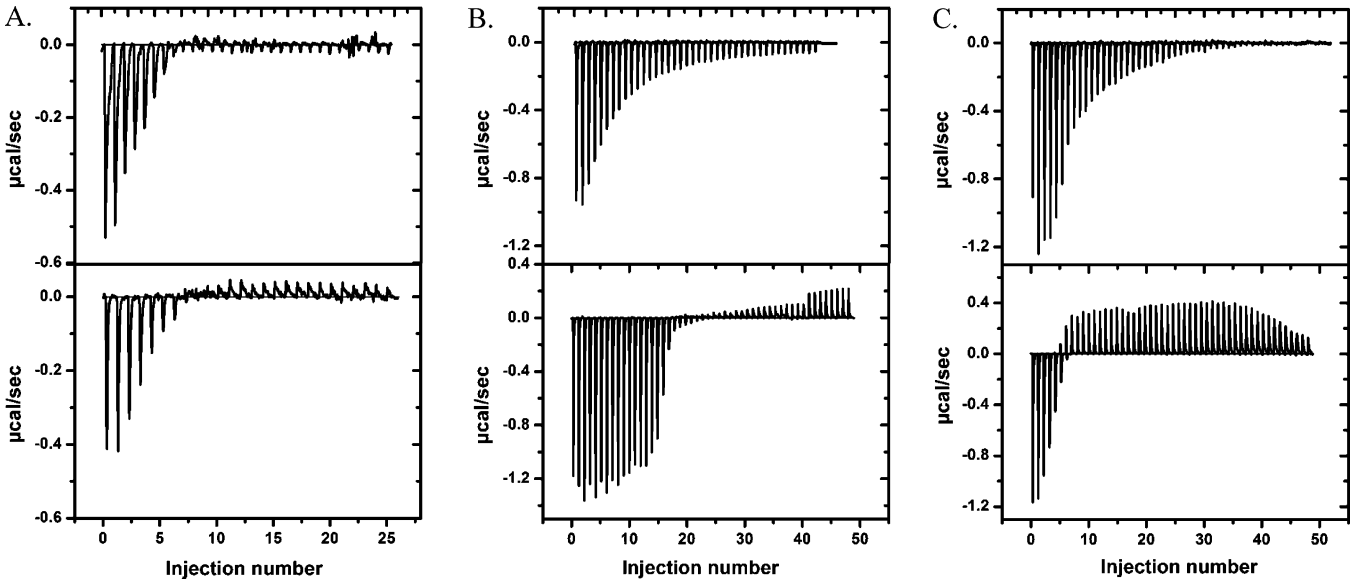

FIGURE 3: Blank-corrected instantaneous heats evolved upon titration of DtxR ancillary site mutants: (A) DtxRΔSH3, (B) H79A, and (C) E83A. In each, the top panel was obtained upon titration with $Ni(II)Cl_2$ and the bottom panel upon titration with $Cd(II)Cl_2$.

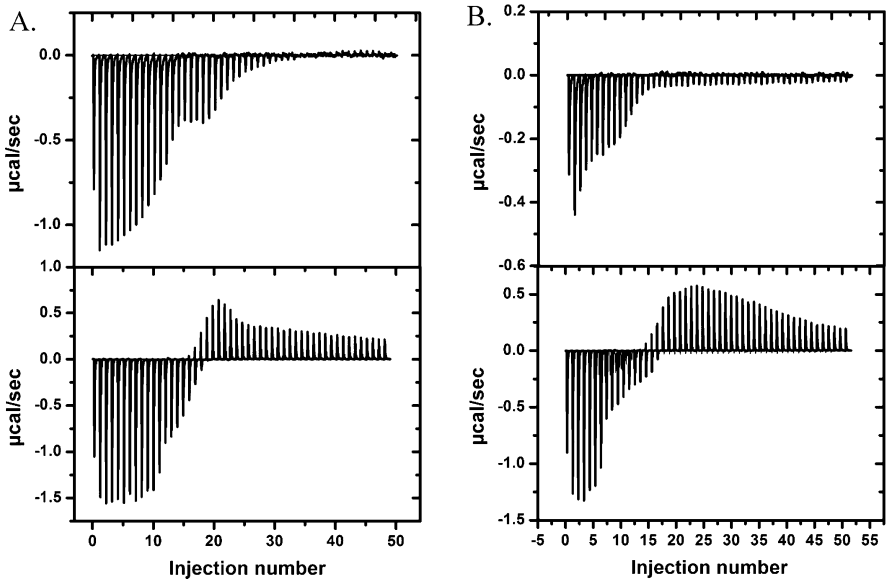

FIGURE 4: Blank-corrected instantaneous heats evolved upon titration of DtxR primary site mutants: (A) M10A and (B) C102A. In each, the top panel was obtained upon titration with $Ni(II)Cl_2$ and the bottom panel upon titration with $Cd(II)Cl_2$.

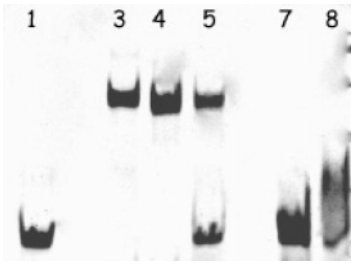

FIGURE 5: Primary site mutants do not bind *tox* DNA. Mobility shift assay comparing DNA binding ability of wild-type and mutant DtxR constructs: lane 1, DNA alone; lane 3, wild-type DtxR; lane 4, DtxRΔSH3; lane 5, H79A; lane 7, C102A; and lane 8, M10A (lanes 2 and 6 were empty). Gel run in the presence of 1 mM $Ni(II)Cl_2$. Each lane contained 90 nM DNA, and all but lanes 1, 2, and 6 contained 2 μM protein.

and holorepressor indicate that metal binding does not induce the formation of significant amounts of new helical structure since there is only a 2−3% increase in helix content (not shown). In contrast, metal binding induces substantial changes in the near-UV CD spectra, and they were used to monitor metal-induced changes in protein tertiary structure. Figure 6A shows the near-UV CD spectrum of wild-type apoDtxR. The spectrum is dominated by a broad, low-intensity ^1L_a transition of tryptophan ($\lambda_{max} \sim 285$ nm) that overlaps with two intense ^1L_b bands ($\lambda_{max} = 287$ and 293.4 nm). The third ^1L_b transition typically associated with tryptophan (*39*) is observed at ~281 nm but is consistently lower in intensity than the other two transitions. Transitions due to tyrosine or phenylalanine residues are much lower in intensity. DtxR contains a single tryptophan, W104, that is present at the dimer interface and is near the primary metal binding site (Figure 1B). Addition of excess Cd(II) to apoDtxR inverted and blue-shifted the ^1L_a transition in a linear fashion until 1.5 equiv of metal had been added, after which there was no further change in this band up to 8 equiv of metal (Figure 6B). The molar ellipticity at 287 nm ($[\Theta]_{287}$)

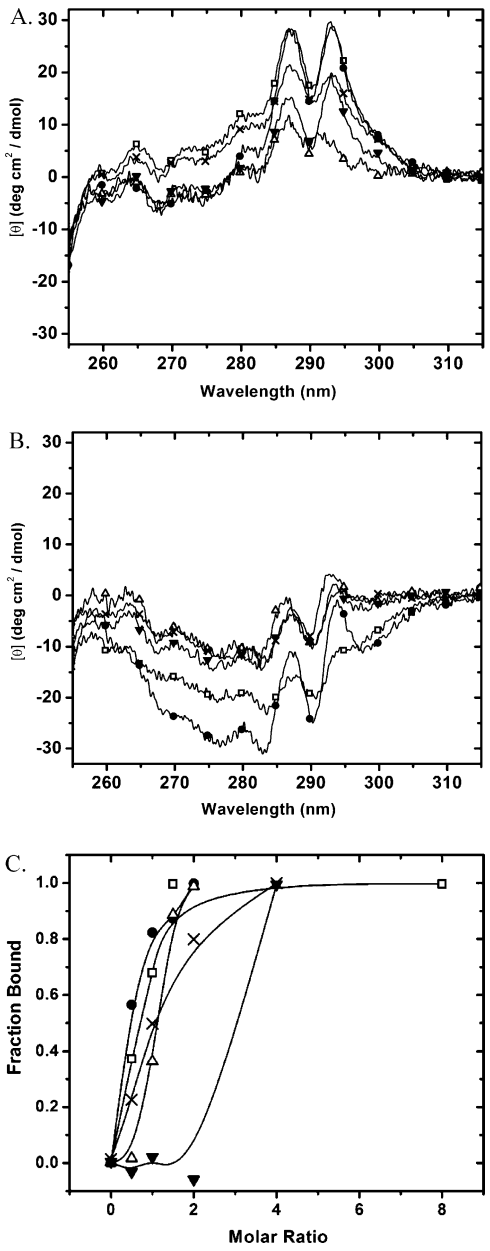

FIGURE 6: Changes in tertiary structure of DtxR upon Cd(II) binding. (A) Near-UV CD spectra of DtxR and binding site mutants in the absence of metal. (B) Near-UV CD spectra of DtxR and binding site mutants in the presence of excess $Cd(II)Cl_2$. (C) Change in molar ellipticity at 287 nm, $[\Theta]_{287}$, as a function of the metal:protein molar ratio. The lines are obtained by b-spline smoothing and do not indicate fitting to a particular model: wild type (□), DtxRΔSH3 (●), H79A (△), M10A (▼), and C102A (×).

of apoDtxR was 28.4 deg cm^2 dmol^{-1}, whereas $[\Theta]_{287}$ was −15.2 deg cm^2 dmol^{-1} at 8 equiv of metal. The ^1L_b transitions exhibited a slight blue shift with an increase in the metal concentration. Near-UV CD spectra collected under identical conditions for Ni(II)-activated DtxR are dominated by Ni(II) transitions and were not used to monitor metal-induced structural changes in the protein environment.

Structure Change in DtxRΔSH3 and Ancillary Site Mutants. Panels A and B of Figure 6 also show near-UV CD spectra for ancillary and primary metal site mutants collected under apo and holo conditions, respectively. Figure 6C shows normalized progress curves indicating the changes in molar ellipticity as a function of added metal. The $[\Theta]_{287}$ values for apo- and holo-DtxRΔSH3 are 28.3 and −11.2 deg cm^2 dmol^{-1}, respectively, similar to that of wild-type DtxR. Addition of Cd(II) to DtxRΔSH3 induced a linear change in $[\Theta]_{287}$ until 1 equiv of metal was added, and then remained constant at higher numbers of metal equivalents. The ^1L_a and ^1L_b transitions for the H79A mutant are weaker than for the wild-type protein ($[\Theta]_{287}$ = 11.95 deg cm^2 dmol^{-1}). Addition of Cd(II) induces roughly linear changes in the ^1L_a transition until 1.5 molar equiv, although the $[\Theta]_{287}$ value at this point (−5.61 deg cm^2 dmol^{-1}) is lower than that of wild-type DtxR. Near-UV CD spectra of E83A were complicated by sample precipitation and are not presented.

Structure Change in Primary Site Mutants. The molar ellipticities of the ^1L_b transitions in apo-C102A and apo-M10A mutants are intermediate between that of the apo wild type and apo H79A proteins (Θ_{287} = 21.7 and 14.6 deg cm^2 dmol^{-1} for M10A and C102A, respectively). Addition of Cd(II) induces linear changes in the ^1L_a transition of C102A until approximately 1.5 equiv of metal with a more gradual decrease observed at higher numbers of equivalents of added metal (Θ_{287} = −1.98 at 4 molar equiv of metal). The Cd(II)-induced structural change in M10A differs substantially from those of the other proteins. Specifically, there is little change in the molar ellipticity of the ^1L_a transition through 2 molar equiv of Cd(II). At higher metal concentrations, the CD spectrum inverted in response to added metal, although the final molar ellipticity is reduced (less negative) than for wild-type DtxR.

Domain−Domain Distances during Metal Activation. Detailed structural studies of apo-DtxR in solution are complicated by extensive microsecond to millisecond conformational averaging of the entire N domain (*21*) that broaden the NMR resonances and prevent sequential chemical shift assignment. In contrast, the backbone resonances of the SH3 domain are well-resolved and readily assigned. The distances expected from residues E170 and Q173 to the primary (and ancillary) site metal are 12.4 (5.8) and 13.0 (6.7) Å, respectively (*18*). To further probe the metal binding sequence, the distance from SH3 domain backbone resonances to the first metal bound to DtxR was determined from the enhancement in longitudinal relaxation rates in the presence of a paramagnetic metal ion [Mn(II)]. Cd(II)-bound DtxR was used as a diamagnetic control for the metal-bound state. Structural studies by Hol's group have established that the metal-activated structure of DtxR is nearly superimposable for Mn(II), Cd(II), Ni(II), Co(II), and Fe(II) (*12*, *17*, *18*). Titrating DtxR with $Mn(II)Cl_2$ yielded a binding isotherm containing the exothermic−endothermic pattern resembling that of wild-type DtxR, indicating that DtxR binds Mn(II) ions in the same order as Ni(II) and Cd(II) (not shown). Figure 7A shows the signal decay for the backbone amide nitrogen of residue E170 of DtxR in the presence 0.8 equiv of Mn(II) or Cd(II), and Figure 7B shows the reduction in T_1 for this residue and for Q173 (which also coordinates the ancillary site metal) and Q178 (which does not). The enhanced relaxation for these and other SH3 domain backbone nitrogen atoms was transformed into distance to the paramagnetic metal using the Solomon−Bloembergen equation (Table 1). The distances from the backbone amide nitrogen of E170 and Q173 to the paramagnetic center are 12.9 and 13.5 Å, respectively, in the presence of 0.8 equiv of metal. Increasing the metal concentration to 1.6 molar

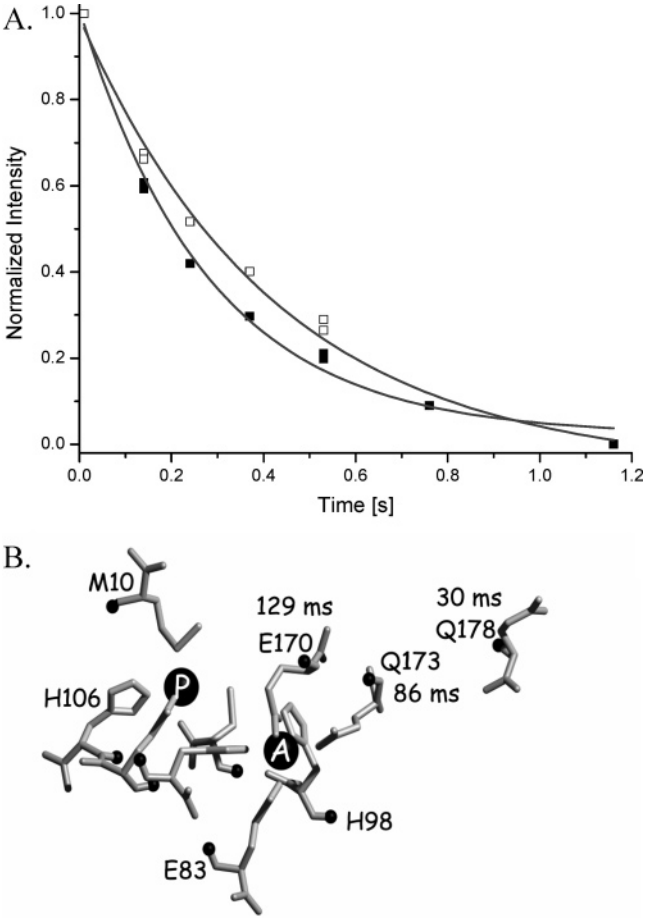

FIGURE 7: Paramagnetic relaxation enhancement in Mn(II)-bound DtxR. (A) Resonance intensity as a function of relaxation delay for ^{15}N nuclei in the presence of 0.8 molar equiv of Mn(II) (■) or Cd(II) (□) for residue E170 of DtxR. (B) Difference in T_1 (in milliseconds) between the Cd(II)- and Mn(II)-bound repressors determined as T_1[Cd(II)] − T_1[Mn(II)] indicated within the structure of the metal-bound repressor. The primary and ancillary metal sites are indicated as solid circles labeled P and A, respectively. The N atoms are depicted as small spheres.

Table 1: Distances from the Metal Center to SH3 Domain Residues

	0.8 equiv		1.6 equiv	
	ΔT_1 (ms)	r (Å)	ΔT_1 (ms)	r (Å)
E170	226	12.9 ± 0.3	230	8.8 ± 0.3
Q173	126	13.5 ± 0.4	270	8.3 ± 0.6
Q178	30	17.6 ± 0.3	30	17.2 ± 0.5

equiv changes the distances to 9.3 and 7.2 Å for these same two residues, respectively. The distance calculated in the 1.6 molar equiv samples reflects enhanced relaxation due to averaging over all bound species. SH3 domain residues not involved in metal binding (for example, Q178) show little enhancement in relaxation rates upon metal binding.

DISCUSSION

Structural studies of apo- and holo-DtxR in the crystalline and solution states provide information about the starting and end points of the activation process. The process starts with the aporepressor as a loosely dimeric species (*22*) containing extensive helical secondary structure, but lacking long-range structural order in the metal- and DNA-binding domain (*21*). The C-terminal SH3-like domain is bound to the proline-rich peptide (Pr) segment that links the N- and C-terminal domains (*30*). Activation by metal increases the affinity for dimer formation by ~100-fold (*22*) and induces a folding transition in the N domain (*21*). The Pr segment is dissociated from the SH3 domain and interacts with the N domain, while the SH3 domain participates in coordinating the ancillary site metal (*18*, *20*).

While there have been many studies characterizing the structure of the apo and holo states, there are few studies on the activation mechanism itself. Here we address the following questions: What is the metal binding affinity, and can the two physical metal binding sites be distinguished energetically? Which of the two metal binding sites is bound first? How is metal binding connected to structure change that leads to activation?

Metal Binding by Wild-Type DtxR. The pattern of heat evolution following Ni(II) or Cd(II) binding by wild-type DtxR is distinctive and indicates a series of metal-induced events, each having a characteristic energetic profile, leading to activation of repressor function (Figure 2). It is readily apparent from these isotherms that metal binding by DtxR is more complicated than binding to two identical, noninteracting sites. Binding isotherms exhibiting the complexity seen for metal binding by DtxR have been reported previously (*40*−*42*), but quantitative analysis is not a trivial task. Given the current state of information regarding metal binding by the DtxR family of proteins, a semiquantitative analysis of the binding isotherms has been performed. No attempt to account explicitly for heat evolution arising from protonation changes, metal-induced changes in dimerization, folding, or cooperative interactions between individual sites was made. The objective was to identify apparent thermodynamic quantities that could be used to parametrize a molecular model for metal activation of DtxR.

As a minimal dissection of the results, we consider the binding isotherm of wild-type DtxR to contain three overlapping heat-evolving processes, as shown in Figure 8A. The two physical metal binding sites in DtxR coordinate metal via a combination of oxygen, nitrogen, and sulfur ligands. Therefore, we expect that binding each of the 2 equiv of metal will be predominantly exothermic (processes I and II in Figure 8A). The endothermic process (process III in Figure 8A) observed in the isotherms must arise from metal-induced burial of hydrophobic surfaces associated with folding of the N domain, including changes in the interactions between the N and SH3 domains. Titrations performed over a 20-fold range of protein concentration indicate that changes in the amount of dimeric protein do not contribute significantly to the endothermic processes.

A binding model based on two independent sites using the binding partition function

$$\Psi = (1 + K_1x)^{n_1} + (1 + K_2x)^{n_2}$$

was modified to analyze the calorimetry data (*43*) and fitted to the integrated heats (Figure 8B) to yield the apparent binding parameters for Ni(II) presented in Table 2. In this model, K_1 (n_1) and K_2 (n_2) are the apparent equilibrium association constants (and stoichiometries) for the two sites. The model identifies a single high-affinity site ($K_{D1} \sim 200$ nM; $n = 1.1$) with enthalpically driven metal binding and a second site of lower affinity ($K_{D2} \sim 1.7$ μM; $n \sim 2$) where

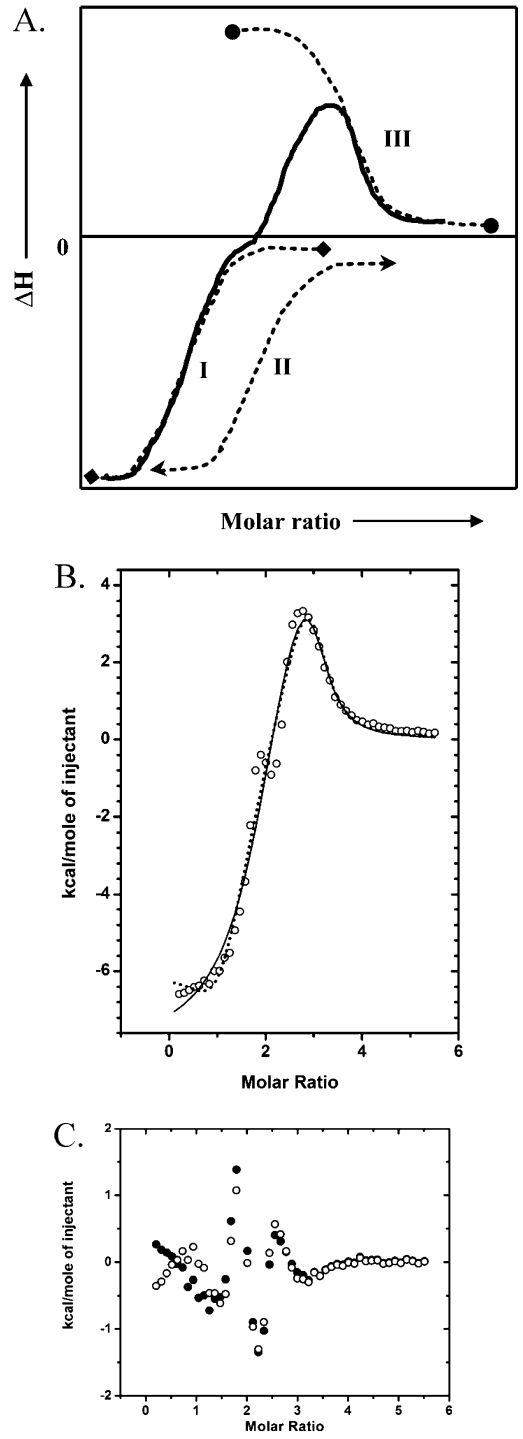

FIGURE 8: Analysis of the Ni(II) binding isotherm for wild-type DtxR. (A) Schematic analysis of the binding isotherm for wild-type DtxR, indicating the decomposition of the observed isotherm into two exothermic and one endothermic components. (B) Integrated heats obtained upon titration of $Ni(II)Cl_2$ into DtxR. The lines represent fits to models for two independent sites (—) and three sequential sites (···). (C) Residuals to the fits: (●) two-site model and (○) three-site model.

the binding is entropically driven (Table 2). These apparent binding affinities are in rough agreement with existing estimates of Ni(II) binding affinity in DtxR (*22*) but clearly resolve separate binding energies. It has previously been pointed out that the two-independent site model is mathematically equivalent to binding models that include cooperative interactions between the two binding sites (*44*).

Table 2: Equilibrium Parameters for Binding of $Ni(II)Cl_2$ to DtxR Obtained from ITC

model	n^a	K_D (μM)^b	ΔH^{app} (kcal/mol)^c	$T\Delta S^{app}$ (kcal/mol)^d
two sites, simultaneous	1.1	0.19 (0.02)	−8.1 (0.6)	1.11 (0.1)
	2.0	1.69 (0.03)	8.9 (0.7)	16.7 (1.2)
three sites, sequential	1	0.16 (0.1)	−6.4 (0.3)	2.9 (0.2)
	1	0.86 (0.4)	−8.6 (0.9)	−0.3 (0.01)
	1	2.31 (1.5)	8.7 (0.8)	16.4 (1.5)

[a] Number of sites (fixed at unity for the three-site, sequential model). [b] Equilibrium dissociation constant (and fitting error). [c] Apparent enthalpy (and fitting error) associated with each binding event. [d] Apparent entropy (and fitting error) at 298 K associated with each binding event.

The metal binding affinity for Cd(II) was not quantified due to complications arising from aggregation at higher metal:protein ratios.

The Ni(II) data were also fit to a model based on three sequential binding sites with binding partition function

$$\Psi = (1 + K_1x)(1 + K_2x)(1 + K_3x)$$

where K_n represents the apparent stoichiometric equilibrium constant for binding a single ligand in each site (Figure 8B and Table 2). The three-sequential site model can also be interpreted in terms of energetic interactions between the sites. Figure 8C shows the residuals for binding to the two-site independent and three-site sequential models. In each case, there are nonrandom deviations of the residuals from zero that indicate additional heat-evolving processes that must be included in a complete binding model, i.e., the dispersive component in the residuals centered at a molar ratio of 2. At this point, we cannot distinguish between the two-independent site and the three-sequential site models because the fits are equally good based on the reduced χ^2 values and they contain the same degrees of freedom (6). Other binding models based on two, three, or four sequential or simultaneous binding sites yielded statistically poorer fits as judged from the residuals and reduced χ^2 values (not shown).

Thus, the ligand binding data suggest the presence of two or three energetically distinct binding sites. At this point, we cannot address the question of cooperativity between the two metal binding sites or between the two monomers of dimeric DtxR. Additional spectroscopic and biophysical studies are under way to further refine the energetics of metal binding, and they will be reported elsewhere. Here we continue our analysis assuming the validity of the simpler, two-independent binding site model.

Metal Binding in Ancillary Site Mutants. The ancillary site metal is coordinated by the side chains of residues H79, E83, H98, E170, and Q173. Mutating any of these residues to Ala reduces repressor activity by up to 50% (*16*, *20*). Given this, it is natural to assume that the ancillary site mutants would bind 1 equiv of metal and represent a half-activated repressor. Our data indicate that each of the ancillary site mutants investigated (H79A, E83A, and DtxRΔSH3) does, indeed, bind 1 equiv of Ni(II), consistent with the stoichiometry detected for H79A previously (*22*). Each ancillary site mutant also binds 1 equiv of Cd(II) with additional weak binding leading to aggregation at high metal:protein ratios. Inspection of the binding isotherms indicates that the Ni(II) binding stoichiometry is close to unity with an apparent binding affinity weaker than that observed for the first

binding process in wild-type DtxR. Furthermore, eliminating metal binding to the ancillary site has altered the binding energetics such that the endothermic binding process is suppressed. The endothermic phase in the binding isotherms indicates that ancillary site coordination results in substantial changes in the exposure of hydrophobic surfaces. This could arise from metal-induced folding of the N domain (*21*), from changes involving the SH3-like domain (*30*), or from both.

Each ancillary site mutant exhibits metal-induced conformational changes in the tryptophan environment that mimic the changes observed in the wild-type protein, indicating that they are sensitive to the same metal binding process. Specifically, the ^1L_a transition in the near-UV CD spectra of DtxRΔSH3 and H79A changes intensity upon binding the first metal equivalent. The molar ellipticity of DtxRΔSH3 is identical to that of the wild type in the apo and holo forms. In contrast, the molar ellipticity of apo-H79A is lower than that of the wild-type protein, indicating that conformational averaging around the tryptophan environment in apo-H79A differs from that of the wild type. A similar spectrum is observed for apo-E83A (not shown). Metal binding effects an inversion of the ^1L_a transition, indicating that metal binding induces a conformational change around the W104 side chain in the ancillary site mutants that is similar to that in the wild type. However, the final molar ellipticity of the metal-bound H79A is lower than that of the wild type, indicating residual flexibility of the tryptophan side chain or an altered conformation in this mutant.

Metal Binding in Primary Site Mutants. The primary metal binding site consists of residues M10, C102, E105, and H106. Mutating any of these residues to Ala abolishes repressor activity (*16*). We anticipated that metal binding would be reduced to (at most) 1 equiv of metal in the two primary site mutants investigated in this study. Instead, we observed that both M10A and C102A bound multiple equivalents of divalent transition metal. Ni(II) binding yields net exothermicity, whereas Cd(II) binding yields a mixed exo- and endothermic response, similar to that of the wild type.

Mutating C102 changes the conformational averaging of the tryptophan side chain slightly on the basis of the reduced molar ellipticity for this mutant. Metal binding effects structural changes similar to that observed in the wild type, although the molar ellipticity of the metal-bound state is weaker than that of the wild type. The tryptophan environment in apo-M10A is similar to that of the wild-type and C102A apoproteins, but there is no change in the environment until 2 molar equiv of metal is added, upon which there is an inversion in the ^1L_a transition, indicating a structural transition toward a more ordered form as seen in the wild type and the other mutant proteins. Thus, metal binding in M10A yielded a structural response fundamentally different from that of the wild type or the other mutant forms.

Despite binding 2 equiv of metal, these mutants were confirmed to be inactive in gel mobility shift assays (Figure 5). An examination of the DtxR structure suggests a possible explanation for this paradoxical result. The helix−turn−helix (HTH) DNA binding subdomain is connected to the metal binding sites and the dimerization interface via a series of salt bridges. Specifically, the E21−R33 salt bridge probably functions to maintain the structural integrity of the HTH subdomain, whereas the E20−R80 salt bridge is important for connecting the DNA binding and dimerization subdomains (lower and upper half of the protein, respectively). Mutating residues involved in these salt bridges perturbs the orientation of the DNA-binding helices and reduces repressor activity almost as much as primary site mutants and more than the ancillary site mutants (*45*). Therefore, we anticipate that the HTH DNA binding subdomain moves as a rigid unit upon metal coordination.

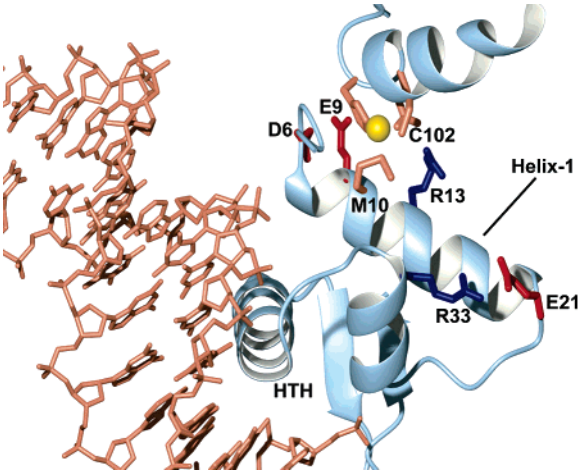

FIGURE 9: Detail of the DNA-bound state, indicating the location of the HTH DNA binding motif relative to the primary metal binding site. Residues D6 and E9 in helix H1 and the E21−R33 salt bridge are indicated.

As shown in Figure 9, the primary metal binding site is adjacent to other acidic residues and to numerous salt bridges that connect the metal binding and DNA binding subdomains. Helix 1 contains two acidic residues that are adjacent to or one helical turn away from M10 (D6 and E9, respectively). Indeed, some of these residues were identified as possible metal coordinating ligands in initial crystal structures of apo-DtxR (*15*, *16*). We propose that metal coordination at the primary site in the M10A or C102A mutant involves these (or other) acidic residues. This "miscoordination" would alter the position of helix 1 and preclude the proper alignment of the helix−turn−helix DNA binding motifs, resulting in an inactive repressor. Further support for this mechanism comes from the different near-UV CD spectra of the primary site mutants compared to the wild-type repressor, which indicate that the metal-bound structures of these proteins are, indeed, different.

Energetic Differences in Binding Ni(II) versus Cd(II). Miscoordination of the primary metal in C102A and M10A mutants might perturb the coordination geometry of the bound metals, which may explain the distinctly different binding isotherms obtained for nickel and cadmium in the primary site mutants. Ni(II) is a d^7 transition ion that prefers binding ligands in a tetracoordinated square planar geometry, although other coordinations and geometries are observed (*46*). In contrast, Cd(II) is a d^{10} ion that binds ligands exclusively in a tetrahedral geometry. These differences are readily apparent in the energetics of coordination. Specifically, we see that the Cd(II) binding isotherm more closely resembles that of the wild type in having both exo- and endothermic portions of the binding curve, whereas the binding of Ni(II) to either primary site mutant does not contain a (net) endothermic phase. The similarity of the wild-type and mutant isotherms for cadmium indicates that this metal is bound without substantial changes in the structure

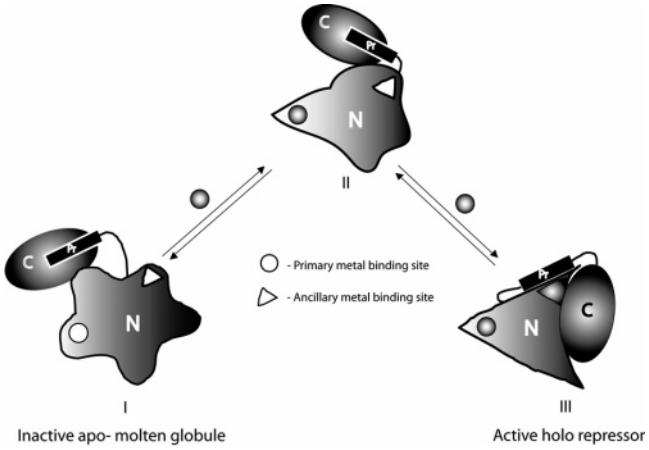

FIGURE 10: Schematic diagram showing the sequence of metal binding and structure change during activation of DtxR by divalent transition metal ions.

of the holoprotein. On the other hand, accommodating the higher coordination geometry for nickel introduces strain into the metal-bound mutant proteins, and probably changes the metal binding affinity, resulting in substantially different energetic profiles for ligand binding by the primary site mutants compared to the wild-type protein.

A Mechanistic Model for Metal Activation of DtxR. The results of this study allow us to propose a mechanism for metal activation that explains the effects of known mutants on repressor function. This mechanism is shown schematically in Figure 10. The first metal equivalent binds to the primary site of DtxR, based on the absence of an endothermic response in all mutants in which the ancillary binding site is compromised. More direct evidence for this assertion was obtained by measuring the distance from the first metal bound to the backbone amides of residues E170 and Q173. As a consequence of metal binding to the primary site, residues in helix H5 and the N-terminal loop following this helix become organized (*13*, *15*). The DNA binding subdomain is connected to the rest of the protein through ligation of M10 in helix H1 (see Figure 1). In addition, salt bridges between E20 and R80 and between E19 and R69 may form at this stage and further consolidate the interactions between the DNA binding and dimerization subdomains.

Metal binding at the primary site also begins to form the native dimer interface through interactions at the extreme amino terminus of DtxR and through H5. In addition, metal-induced folding of the H5 helix would alter the tryptophan environment due either to helix formation or to rotation of the helix toward its position seen in the activated form of the protein. This altered environment is reflected in the metal-dependent changes in the near-UV CD spectrum observed in DtxR. We see an immediate change in the polarization of the ^1L_a transition in W104 coupled with a slight blue shift, consistent with a metal-induced change to a less polar environment and changes in the side chain rotamer population.

The second metal binding event occurs at the ancillary site, which involves residues in helices H4, H5, and H8 (in the SH3-like domain; see Figure 1). Binding the second metal equivalent fixes the position of these helices. This completes the folding of the N domain and the formation of the native dimer interface, resulting in a substantial enhancement in dimer affinity in the metal-activated state (*22*). The burial of hydrophobic residues and changes in the SH3 domain upon coordination of the metal via residues E170 and Q173 contribute to the endothermic phase of the wild-type binding isotherm.

This model explains the observed primary and ancillary site mutant phenotypes. The key event in activation is primary site binding, which aligns the DNA binding helices and enhances dimer formation. Ancillary site mutants still bind metal at the primary site and align the DNA binding helices, but repressor function is inhibited compared to that of the wild-type protein, either because the DNA binding helices are not optimally aligned or because the dimer interface is weaker (or both). In contrast, primary site mutants are nonfunctional because the DNA binding helices are not aligned in an orientation that supports binding to the *tox* promoter.

The mechanism proposed here provides insights into the basis for hyperactivity in the E175K mutant (*11*). This form of DtxR appears to be active at lower metal concentrations, indicating either a reduced requirement for metal or an enhanced metal binding affinity (*10*). We previously suggested that this mutant functions by establishing salt bridges with residues in the dimerization subdomain of the N domain. On the basis of the results of this study, we anticipate that this would have the effect of increasing metal binding affinity in the primary site. Experiments designed to test this and other aspects of the proposed mechanism are currently underway and will be reported elsewhere.

REFERENCES

1. Hantke, K. (2001) Iron and metal regulation in bacteria, *Curr. Opin. Microbiol. 4*, 172−177.
2. Braun, V. (2001) Iron uptake mechanisms and their regulation in pathogenic bacteria, *Int. J. Med. Microbiol. 291*, 67−79.
3. Ratledge, C., and Dover, L. G. (2000) Iron metabolism in pathogenic bacteria, *Annu. Rev. Microbiol. 54*, 881−941.
4. Boyd, J., Oza, M. N., and Murphy, J. R. (1990) Molecular cloning and DNA sequence analysis of a diphtheria *tox* iron-dependent regulatory element (*dtxR*) from *Cornybacterium diptheriae*, *Proc. Natl. Acad. Sci. U.S.A. 87*, 5968−5972.
5. Schmitt, M. P., Predich, M., Doukhan, L., Smith, I., and Holmes, R. K. (1995) Characterization of an iron-dependent regulatory protein (IdeR) of *Mycobacterium tuberculosis* as a functional homolog of the diphtheria toxin repressor (DtxR) from *Corynebacterium diphtheriae*, *Infect. Immun. 63*, 4284−4289.
6. Gold, B., Rodriguez, G. M., Marras, S. A., Pentecost, M., and Smith, I. (2001) The *Mycobacterium tuberculosis* IdeR is a dual functional regulator that controls transcription of genes involved in iron acquisition, iron storage and survival in macrophages, *Mol. Microbiol. 42*, 851−865.
7. Posey, J. E., Hardham, J. M., Norris, S. J., and Gherardini, F. C. (1999) Characterization of a manganese-dependent regulatory proteins, TroR, from *Treponema pallidum*, *Proc. Natl. Acad. Sci. U.S.A. 96*, 10887−10892.
8. Jakubovics, N. S., Smith, A. W., and Jenkinson, H. F. (2000) Expression of the virulence-related Sca (Mn^{2+}) permease in *Streptococcus gordonii* is regulated by a diphtheria toxin metallorepressor-like protein ScaR, *Mol. Microbiol. 38*, 140−153.
9. Que, Q., and Helmann, J. D. (2000) Manganese homeostasis in *Bacillus subtilis* is regulated by MntR, a bifunctional regulatory related to the diphtheria toxin repressor family of proteins, *Mol. Microbiol. 35*, 1454−1468.
10. Love, J. F., vanderSpek, J. C., Marin, V., Guerrero, L., Logan, T. M., and Murphy, J. R. (2004) Genetic and biophysical studies of diphtheria toxin repressor (DtxR) and the hyperactive mutant DtxR(E175K) support a multistep model of activation, *Proc. Natl. Acad. Sci. U.S.A. 101*, 2506−2511.
11. Sun, L., VanderSpek, J., and Murphy, J. R. (1998) Isolation and characterization of iron-independent positive dominant mutants

of the diphtheria toxin repressor DtxR, *Proc. Natl. Acad. Sci. U.S.A. 95*, 14985−14990.
12. Manabe, Y. C., Saviola, B. J., Sun, L., Murphy, J. R., and Bishai, W. R. (1999) Attenuation of virulence in *Mycobacterium tuberculosis* expressing a constitutively active iron repressor, *Proc. Natl. Acad. Sci. U.S.A. 96*, 12844−12848.
13. Qiu, X., Verlinde, C. L. M. J., Zhang, S., Schmitt, M. P., Holmes, R. K., and Hol, W. G. J. (1995) Three-dimensional structure of the diphtheria toxin repressor in complex with divalent cation corepressors, *Structure 3*, 87−100.
14. Pohl, E., Holmes, R. K., and Hol, W. G. J. (1998) Motion of the DNA-binding domain with respect to the core of the diphtheria toxin repressor (DtxR) revealed in the crystal structure of apo- and holo-DtxR, *J. Biol. Chem. 273*, 22420−22427.
15. Schiering, N., Tao, X., Zeng, H., Murphy, J. R., Petsko, G. A., and Ringe, D. (1995) Structures of the apo- and metal ion-activated forms of the diphtheria *tox* repressor from *Corynebacterium diphtheriae*, *Proc. Natl. Acad. Sci. U.S.A. 92*, 9843−9850.
16. Ding, X., Zeng, H., Schiering, N., Ringe, D., and Murphy, J. R. (1996) Identification of the primary metal ion-activation sites of the diphtheria tox repressor by X-ray crystallography and site-directed mutagenesis, *Nat. Struct. Biol. 3*, 382−387.
17. Qiu, X., Pohl, E., Holmes, R. K., and Hol, W. G. J. (1996) High-resolution structure of the diptheria toxin repressor complexed with cobalt and manganese reveals an SH3-like third domain and suggests a possible role of phosphate as co-corepressor, *Biochemistry 35*, 12292−12302.
18. Pohl, E., Holmes, R. K., and Hol, W. G. J. (1999) Crystal structure of a cobalt-activated diphtheria toxin repressor-DNA complex reveals a metal-binding SH3-like domain, *J. Mol. Biol. 292*, 653−667.
19. Wang, G., Wylie, G. P., Twigg, P. D., Caspar, D. L. D., Murphy, J. R., and Logan, T. M. (1999) Solution structure and peptide binding studies of the C-terminal Src homology 3-like domain of the diphtheria toxin repressor protein, *Proc. Natl. Acad. Sci. U.S.A. 96*, 6119−6124.
20. Love, J. F., VanderSpek, J. C., and Murphy, J. R. (2003) The src homology 3-like domain of the diphtheria toxin repressor (DtxR) modulates repressor activation through interaction with the ancillary metal ion-binding site, *J. Bacteriol. 185*, 2251−2258.
21. Twigg, P. D., Parthasarathy, G., Guerrero, L., Logan, T. M., and Caspar, D. L. (2001) Disordered to ordered folding in the regulation of diphtheria toxin repressor activity, *Proc. Natl. Acad. Sci. U.S.A. 98*, 11259−11264.
22. Spiering, M. M., Ringe, D., Murphy, J. R., and Marletta, M. A. (2003) Metal stoichiometry and functional studies of the diphtheria toxin repressor, *Proc. Natl. Acad. Sci. U.S.A. 100*, 3808−3813.
23. Tao, X., and Murphy, J. R. (1992) Binding of the metaolloregulatory protein DtxR to the diptheria *tox* operator requires divalent heavy metal ion and protects the palindromic sequence from DNase I digestion, *J. Biol. Chem. 267*, 21761−21764.
24. Tao, X., Boyd, J., and Murphy, J. R. (1992) Specific binding of the diptheria *tox* regulatory element DtxR to the *tox* operator requires divalent heavy metal ions and 9-base-pair interrupted palindromic sequence, *Proc. Natl. Acad. Sci. U.S.A. 89*, 5897−5901.
25. Schmitt, M. P., and Holmes, R. K. (1993) Analysis of diphtheria toxin repressor-operator interactions and characterization of a mutant repressor with decreased binding activity for divalent metal, *Mol. Microbiol. 9*, 173−181.
26. Pohl, E., Qiu, W., Must, L. M., Holmes, R. K., and Hol, W. G. J. (1997) Comparison of high-resolution structures of the diphtheria toxin repressor in complex with cobalt and zinc at the cation−anion binding site, *Protein Sci. 6*, 1114−1118.
27. Wang, Z., Schmitt, M. P., and Holmes, R. K. (1994) Characterization of mutations that inactivate the diphtheria toxin repressor gene (*dtxR*), *Infect. Immun. 62*, 1600−1608.
28. Tao, X., Zeng, H. Y., and Murphy, J. R. (1995) Transition metal ion activation of DNA binding by the diptheria *tox* repressor requires the formation of stable homodimers, *Proc. Natl. Acad. Sci. U.S.A. 92*, 6803−6807.
29. Love, J. F., and Murphy, J. R. (2002) Design and development of a novel genetic probe for the analysis of repressor-operator interactions, *J. Microbiol. Methods 51*, 63−72.
30. Wylie, G. P., Rangachari, V., Bienkiewicz, E. A., Marin, V., Bhattacharya, N., Love, J. F., Murphy, J. R., and Logan, T. M. (2005) Prolylpeptide binding by the prokaryotic SH3-like domain of the diphtheria toxin repressor: A regulatory switch, *Biochemistry 44*, 40−51.
31. Edelhoch, H. (1967) Spectroscopic determination of tryptophan and tyrosine in proteins, *Biochemistry 6*, 1948−1954.
32. Kay, L. E., Keifer, P., and Saarinen, T. (1992) Pure absorption gradient enhanced heteronuclear single quantum correlation spectroscopy with improved sensitivity, *J. Am. Chem. Soc. 114*, 10663−10665.
33. Farrow, N. A., Muhandiram, R., Singer, A. U., Pascal, S. M., Kay, C. M., Gish, G., Shoelson, S. E., Pawson, T., Forman-Kay, J. D., and Kay, L. E. (1994) Backbone dynamics of a free and phosphopeptide-complexed Src homology 2 domain studied by ^{15}N NMR relaxation, *Biochemistry 33*, 5984−6003.
34. Delaglio, F., Grzesiek, S., Vuister, G. W., Zhu, G., Pfeifer, J., and Bax, A. (1995) NMRPipe: A multidimensional spectra processing system based on UNIX pipes, *J. Biomol. NMR 6*, 277−293.
35. Johnson, B. A., and Blevins, R. A. (1994) NMRView: A computer program for the visualization and analysis of NMR data, *J. Biomol. NMR 4*, 603−614.
36. Bertini, I., Turano, P., and Vila, A. J. (1993) Nuclear magnetic resonance of paramagnetic metalloproteins, *Chem. Rev. 93*, 2833−2932.
37. Tao, X., and Murphy, J. R. (1993) Cysteine-102 is positioned in the metal binding activation site of the *Cornyebacterium diptheriae* regulatory element DtxR, *Proc. Natl. Acad. Sci. U.S.A. 90*, 8524−8528.
38. Wisedchaisri, G., Holmes, R. K., and Hol, W. G. (2004) Crystal structure of an IdeR-DNA complex reveals a conformational change in activated IdeR for base-specific interactions, *J. Mol. Biol. 342*, 1155−1169.
39. Strickland, E. H., and Billups, C. (1973) Oscillator strengths of the ^1L_a and ^1L_b absorption bands of tryptophan and several other indoles, *Biopolymers 12*, 1989−1995.
40. Prorok, M., and Castellino, F. J. (1998) Thermodynamics of binding of calcium, magnesium, and zinc to the *N*-methyl-D-aspartate receptor ion channel peptidic inhibitors, conantokin-G and conantokin-T, *J. Biol. Chem. 273*, 19573−19578.
41. Gilli, R., Lafitte, D., Lopez, C., Kilhoffer, M., Makarov, A., Briand, C., and Haiech, J. (1998) Thermodynamic analysis of calcium and magnesium binding to calmodulin, *Biochemistry 37*, 5450−5456.
42. Birnbaum, D. T., Dodd, S. W., Saxberg, B. E., Varshavsky, A. D., and Beals, J. M. (1996) Hierarchical modeling of phenolic ligand binding to 2Zn−insulin hexamers, *Biochemistry 35*, 5366−5378.
43. Wiseman, T., Williston, S., Brandts, J. F., and Lin, L.-N. (1989) Rapid measurement of binding constants and heats of binding using a new titration calorimeter, *Anal. Biochem. 179*, 131−137.
44. Bains, G., and Freire, E. (1991) Calorimetric determination of cooperative interactions in high affinity binding processes, *Anal. Biochem. 192*, 203−206.
45. Pohl, E., Goranson-Siekierke, J., Choi, M. K., Roosild, T., Holmes, R. K., and Hol, W. G. (2001) Structures of three diphtheria toxin repressor (DtxR) variants with decreased repressor activity, *Acta Crystallogr. D57*, 619−627.
46. Rulisek, L., and Vondrasek, J. (1998) Coordination geometries of selected transition metal ions (Co^{2+}, Ni^{2+}, Cu^{2+}, Zn^{2+}, Cd^{2+}, and $Hg^{2+/-}$) in metalloproteins, *J. Inorg. Biochem. 71*, 115−127.

BI047825W